Numerical solution of surface plasmon polariton mode propagating on spatially periodic metal–dielectric interface

Xue Feng,[1,2] Weiwei Ke,[1] Xuan Tang,[1] Yidong Huang,[1,3] Wei Zhang,[1] and Jiangde Peng[1]

[1] *State Key Laboratory of Integrated Optoelectronics, Department of Electronic Engineering, Tsinghua University, Beijing 100084, China*

[2] *x-feng@tsinghua.edu.cn*

[3] *yidonghuang@tsinghua.edu.cn*

Received March 3, 2009; revised May 15, 2009; accepted May 21, 2009; posted May 26, 2009 (Doc. ID 108276); published June 19, 2009

To obtain the numerical solution of normal surface plasmon polariton (SPP) modes of free oscillations of the electromagnetic field on a cylindrical periodic dielectric–metal interface, a combination method is proposed by taking advantage of Green's function method and Chandezon's approach. With such methods, the dispersion curves and electromagnetic field distributions of SPP modes are calculated based on an Au-Si_3N_4 interface with both sinusoidal and symmetrical sawtooth shapes. The simulation results prove that the proposed method can be applied for calculating the electromagnetic field distribution of the SPP mode at an arbitrary wave vector along the dispersion curve and on arbitrary interface shapes. Furthermore, good stability and sufficient accuracy can be obtained with moderate frequency searching steps and a coefficients matrix order. © 2009 Optical Society of America

OCIS codes: 240.0240, 240.5420, 240.6680.

1. INTRODUCTION

A surface plasmon polariton (SPP) is a transverse-magnetic surface electromagnetic excitation that propagates in a wavelike fashion along the metal and dielectric interfaces [1,2]. When the SPP wave propagates on a spatially periodic metal–dielectric interface, just like the photonic band gap (PBG) in spatially periodic dielectric structures called photonic crystals [3], an energy bandgap for the SPP (SPPBG) can also occur, where propagation of the SPP mode over some range of energies is forbidden [4,5]. This kind of structure with a spatially periodic metal–dielectric interface can be called a surface polaritonic crystal or SPP crystal [2]. Different from an optical wave, the SPP represents quasi-two-dimensional waves with amplitudes decaying exponentially into both of the neighbor media while the field distribution is close to the interface [6]. These unique characteristics make the SPP very promising in some new functional devices, such as resonant absorbers and reflectors [7–9] and biosensor [10,11] or SPP-assisted emission enhancement devices [12–14]. Due to the effect of an SPPBG, SPP crystals provide a new approach for guiding and manipulating SPP waves, which is very useful in new functional devices based on the SPP.

Calculating and analyzing the SPP mode propagating on a spatially periodic metal–dielectric interface, including field and surface charge distributions, is essential to reveal SPPBG-related physical phenomena and to design the proper device structure, such as for the research of SPP-based surface-enhanced Raman scattering, second-harmonic generation, as well as quantum electrodynamics effects, especially for spontaneous emission lifetime modification [15]. Here, not only should the dispersion relation of SPP modes be clarified, but also their field distributions.

One- and two-dimensional SPP crystals have recently been intensively studied [2]. Several theoretical approaches have been devoted to describe the SPPBG and to calculate how the gap width and central position depend upon the grating profile and the amplitude of the modulation. These approaches can be divided into four categories, and a short review of them can be found in [16]. Unfortunately, none of them can be used to obtain the full SPP mode solution, including both the dispersion relation and the field distribution, for the SPP crystal. Among them, the Green' function method (GFM) based on Rayleigh expansion [1,2] is the most popular method. It is widely adopted to investigate the SPP-to-SPP interaction, namely the scattering problem, in a surface periodic structure [17–19]. When the normal SPP modes of free oscillations of the electromagnetic field on the SPP crystal are concerned, however, it is a homogeneous problem rather than a scattering problem, since there is no scattering of a volume or surface electromagnetic wave from the interface [2]. In such a homogeneous problem, even if the dispersion relation of the SPP mode can be well calculated by GFM for both one- and two-dimensional periodic surface profiles [1,2,20–22], field distribution is hard to obtain. On the other hand, Chandezon's approach (CDA) is superior to the Rayleigh expansion method for constructing the electromagnetic field distribution in two-dimensional expansion form [23], but it is hard to use to calculate the dispersion relation. By using the framework of CDA, Barnes *et al.* proposed a perturbation approach to

find analytic expressions for the spatial field and surface charge distributions, and they used it to find the physical origin of SPPBG successfully [16]. However, this method can be used only for calculating the field and surface charge distributions at the Brillouin boundary and can hardly be applied for dispersion relation calculation at an arbitrary wave vector.

In this paper, by taking advantage of GFM and CDA, a combination method is proposed to obtain the numerical solution of an SPP mode propagating on a cylindrical periodic dielectric–metal interface. With the proposed method, the electromagnetic field distribution of the SPP mode at an arbitrary wave vector along the dispersion curve and on an arbitrary interface profile can be calculated. As examples, the dispersion curves and electromagnetic field distributions of the SPP mode are presented based on an Au-Si_3N_4 interface with sinusoidal and symmetrical sawtooth shape functions. Furthermore, the calculating stability of the proposed method is also discussed by comparing the field distribution obtained with different frequency searching steps. According to the results, the proposed method is stable and convenient since only moderate frequency steps and coefficients matrix orders are required to obtain sufficient accuracy. Although the simplest case of periodic dielectric–metal interface is concerned in this paper, we believe that the proposed method can be also extended to more general cases such as two-dimensional or multicoated structures, as it has been proved that the GFM can be applied on two-dimensional periodic surface profiles [2,21,22] and the CDA also can be applied on multicoated structures [23].

The paper is organized as follows. In Section 2, a combination method is proposed by taking advantage of the GFM and CDA. Consequently, the detailed process is demonstrated in two steps of calculating the dispersion relation and the field distribution. In Section 3, the proposed method is applied for calculating the SPP mode on an Au-Si_3N_4 interface with sinusoidal and symmetrical sawtooth shape functions. The calculating stability is also discussed. Section 4 provides a summary.

2. THEORETICAL MODEL AND APPROACH

As shown in Fig. 1, the interface shape is described as $z=s(x)$ with a period of a. The interface consists of a dielectric with a dielectric constant ε_D in the region $z>s(x)$ and a metal in the region $z<s(x)$. The metal is characterized by a real, isotropic, and frequency dielectric function of $\varepsilon_M(\omega)$. Our objective is to find the field and surface charge distributions of SPP modes that satisfy Maxwell's equations and the boundary condition of the periodic dielectric–metal interface shown in Fig. 1.

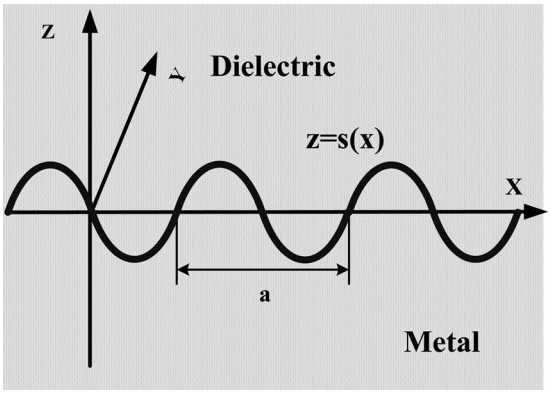

Fig. 1. Schematic cylindrical periodic dielectric–metal interface and reference coordinate system.

As is known, GFM is suitable to calculate the dispersion curve [1,2,20–22], while the cost of computation for field distribution would be very great. CDA is very difficult to apply to calculating the dispersion relation but is superior to the Rayleigh expansion for constructing the electromagnetic field distribution [23], so long as the wave vector k and frequency ω are both known from the dispersion relation. Therefore, taking advantage of GFM and CDA in a combination method is proposed here to obtain the numerical solution of an SPP mode propagating on a cylindrical periodic dielectric–metal interface.

Since the SPP mode is a transverse magnetic (TM or p-polarized) wave, we are only interested in the TM solution of Maxwell's equations. In our reference coordinate system shown in Fig. 1, the magnetic field of the SPP mode contains the field components perpendicular to the symmetry plane, i.e., the y component. Since the interface is symmetrical along the y axis, the magnetic field will also be symmetrical along y axis and can be written as

$$\vec{H}(x,y,z|\omega)=\vec{y}\cdot H_y(x,z|\omega)\exp(-i\omega t)\ . \tag{1}$$

To find the SPP mode solution in the x direction across the interface of $z=s(x)$ and also which amplitudes decay exponentially along the z direction, the process is divided into two steps for calculating the dispersion relation and the field distribution.

A. Calculating the Dispersion Relation

According to GFM, the SPP mode solution can be deduced from the Helmholtz equations by using Eq. (1) and Maxwell's equations, then expanded as Fourier sums that possess the Bloch periodicity property as [1,2,20]

$$H_y(x,z|\omega)=\sum_{n=-\infty}^{+\infty}A_n\exp(i\beta_n z)\exp[i(k_x+nK_g)x]\ , \tag{2}$$

where k_x and A_n are the SPP mode wave vector in the x direction and the field expansion coefficients, respectively. $K_g=2\pi/a$ is the Bragg wave vector of the interface. A series of wave vectors for SPP mode β_n are given by

$$\beta_n=\left[\left(k_x+n\frac{2\pi}{a}\right)^2-\varepsilon\frac{\omega^2}{c^2}\right]^{1/2}. \tag{3}$$

In Eqs. (2) and (3),

$$\varepsilon=\begin{cases}\varepsilon_D, z>s(x)\\ \varepsilon_M(\omega), z<s(x)\end{cases}\quad\text{and}\quad H_y=\begin{cases}H_y^D, z>s(x)\\ H_y^M, z<s(x)\end{cases}$$

represent the dielectric permittivity and the magnetic field in the appropriate medium (metal and dielectric), respectively.

The boundary conditions are satisfied by assuming that the expressions for the fields in the two half spaces are

valid all the way to the interface, which is the Rayleigh hypothesis. The expansion of Eq. (2) is also called the Rayleigh expansion.

By adopting Green's second integral theorem, the problem can be simplified by working only with the field in the dielectric, and a set of integral equations satisfied by the coefficients $\{A_n\}$ can be obtained:

$$\sum_n \frac{k_m k_n + \beta_m^M \cdot \beta_n^D}{i(\beta_m^M - \beta_n^D)} \cdot \frac{1}{a} \int_0^a dx \cdot \exp\left[-i\frac{2\pi}{a}(m-n)x \right] \exp\{i[\beta_m^M - \beta_n^D] \cdot s(x)\} \cdot A_n = 0$$

$$m = 0, \pm 1, \pm 2, \ldots \quad (4)$$

where β_m^M and β_n^D represent the SPP mode wave vector in dielectric and metal, respectively.

To apply the numerical calculation, Eq. (4) need to be truncated to a finite term, i.e., given from $m,n = 0, \pm 1, \pm 2, \ldots, \pm N$. Then Eq. (4) can be presented as a matrix $[M_{m,n}]$ multiplying a column vector $[A_n]$:

$$[M_{m,n}(\omega, k_x, \varepsilon_D, \varepsilon_M, s(x))] \cdot [A_n] = 0 \; . \quad (5)$$

From Eq. (5), it can be easily seen that the elements of the coefficient matrix $[M_{m,n}]$ are related to the frequency ω and wave vector k_x of the SPP mode. Then the dispersion relation between ω and k can be calculated by equating the determinant of the coefficients matrix $[M_{m,n}]$ to zero [1,2,20].

In principle, after the dispersion relation is obtained the expansion coefficient A_n can be solved by substituting the value of ω and k into Eq. (5); therefore, the field distribution can be obtained. However, it is very difficult to obtain the exact value of ω and k to satisfy $\det[M]=0$ in a practical numerical calculation process. Matrix $[M]$ is an ill-conditioned matrix and the absolute value of each element in $[M_{m,n}]$ is quite different.

Using the example of numerical calculation shown in [20], the above statement can be represented. First, we duplicated the calculation of the dispersion curves using the same parameters in [20], where the interface consists of a free-electron metal and vacuum ($\varepsilon_D=1$) with sinusoidal shape function $s(x)=d\cdot\sin(2\pi/ax)$. The period and depth are $a=500$ nm and $d=50$ nm, respectively. The dielectric function of metal was set as $\varepsilon_M(\omega)=1-\omega_p^2/\omega^2$, $h\omega_p=2$ eV. The dimension of the coefficient matrix was truncated to 42×42 ($N=20$) and the step of ω varying was set as $\omega_{\text{step}}=10^{-4}$ eV. The simulation results shown in Fig. 2(a) are well consistent with those in [20], where the energy band gap can be observed clearly. By substituting the results shown in Fig. 2(a) into Eq. (5), the value of $\det[M]$ was calculated at each wave vector. Unfortunately, it was found that the minimum of $|\det[M]|$ is more than 10^{304} as shown in Table. 1. Obviously, it is too huge to be used to calculate the expansion coefficient A_n.

We find that the difference between the absolute value of each element $abs(M_{m,n})$ is very significant. For example, when $k=\pi/a$ and $\omega=1.14$ eV (upper frequency), the maximum and minimum values of $abs(M_{m,n})$ are 1.68×10^{8} and 3.15×10^{-124}, respectively. This is why we stated that $[M]$ is an ill-conditioned matrix, and the value

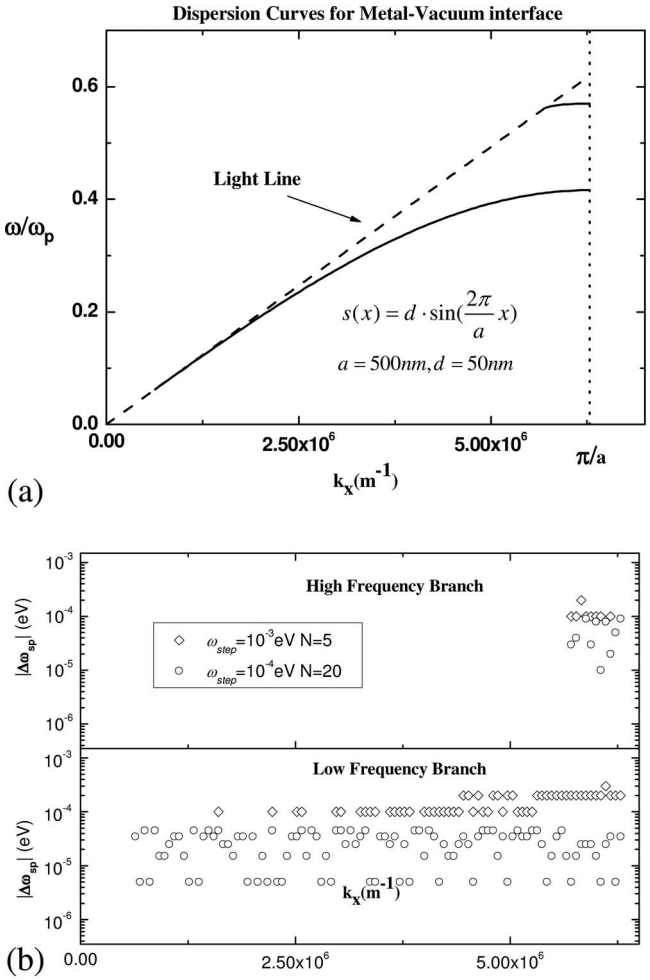

Fig. 2. Calculated dispersion curves with (a) searching step $\omega_{\text{step}}=10^{-4}$ eV and matrix order 42×42, $N=20$ and (b) difference of the SPP mode frequency by reducing ω_{step} to 10^{-5} eV ($N=20$) and reducing N to 5 ($\omega_{\text{step}}=10^{-4}$ eV) for sinusoidal metal–vacuum interface with period $a=500$ nm and depth $d=50$ nm.

of $|\det[M]|$ cannot be reduced by normalizing the matrix elements, even to reduce the searching step ω_{step} or the matrix order N. We recalculated the dispersion curve shown in Fig. 2(a) by reducing ω_{step} to 10^{-5} eV for $N=20$ and reduced the matrix order to $N=5$ for $\omega_{\text{step}}=10^{-4}$ eV. According to the calculation results, the difference of the frequency ($|\Delta\omega_{\text{spp}}|$) compared to that of Fig. 2(a) (where $\omega_{\text{step}}=10^{-4}$ eV, $N=20$) at each k are plotted in Fig. 2(b) with circle and diamond, respectively. The maximum of $|\Delta\omega_{\text{spp}}|$ and minimum of $|\det[M]|$ for both branches are summarized in Table. 1. It can be seen that when ω_{step} is reduced to 10^{-5} eV, $\min|\det[M]|$ can be reduced only to 5.74×10^{302}. Meanwhile, we should notice the fact that the absolute frequency differences $|\Delta\omega_{\text{spp}}|$ are all less than 10^{-3} eV when decreasing ω_{step} from 10^{-4} eV to 10^{-5} eV. It means that further reducing ω_{step} is not necessary to calculate the dispersion curve. On the other hand, it can also be found that $|\Delta\omega_{\text{spp}}|$ are all less than 10^{-3} eV when the matrix order was reduced to $N=5$, even though $\min|\det[M]|$ can be reduced to 2.57×10^{73} in this case, which is still too large.

To overcome it, we try to propose a new method to expand the SPP mode solution in a different form rather

Table 1. Summary for the Maximum Difference of the SPP Mode Frequency ($\Delta|\omega_{spp}|$) and the Minimum Determinant Value of the Coefficient Matrix ($|\det[M]|$) with Different Searching Steps and the Matrix Order

Metal–Vacuum Interface	N	ω_{step} (eV)	$\max\|\Delta\omega_{spp}\|$ (eV)		min $\|\det[M]\|$
			Upper Branch	Lower Branch	
$s(x)=d\cdot\sin(2\pi/ax)$	20	0.0001	\	\	1.03×10^{304}
$a=500$ nm, $d=50$ nm	20	0.00001	9×10^{-5}	4.5×10^{-5}	5.74×10^{302}
	5	0.0001	2×10^{-4}	3×10^{-4}	2.57×10^{73}

than Rayleigh expansion so that a new set of equations, different from Eq. (5), could be obtained to solve the electromagnetic field distribution with the known dispersion relation. Just CDA can be used to achieve this purpose.

B. Calculating the Field Distribution

According to CDA, which is based on a coordinate transformation technique to make the interface flat, the SPP mode solution can be expanded in a two-dimensional expansion form [16,23]:

$$H_y(x,z)=\frac{1}{Z_0}\sum_m\sum_q f_m^q\exp[i\lambda^q(z-s(x))]\times\exp\left[i\left(k+m\frac{2\pi}{a}\right)x\right], \quad (6)$$

where λ^q is the eigenvalues of the mode and f_m^q is the amplitude of the mth Fourier component of the H_y field in the qth eigenmode. The detailed process of CDA can be found in [16,23].

From Eq. (6) we can easily find that the mode solution contains the shape information of interface, not only in the term of $\exp[i\lambda^q(z\text{-}s(x))]$ but also in the eigenvalues λ^q and coefficients f_m^q. This should be contrasted with the mode solution form in GFM, Eq. (2) (Rayleigh expansion), where the equivalent of the eigenvalues are the wave vectors, $\beta_n=[(k_x+n2\pi/a)^2-\varepsilon\omega^2/c^2]^{1/2}$, which are independent of the surface profile. Thus the terms of Fourier summation to evaluate the relevant fields based on CDA are fewer than those based on Rayleigh expansion, i.e., GFM [16]. Furthermore, the SPP mode solution of CDA is very insensitive to the accuracy of the dispersion relation due to the two-dimensional expansion form of the electromagnetic field, which will be discussed more deeply in Section 3. In a word, CDA is superior for constructing the electromagnetic field distribution. Taking the advantages of GFM and CDA, a convenient method to obtain the full SPP mode solution is proposed as follows.

1. Use the rectangle coordinate system x,y,z and calculate the coefficient matrix $[M]$ as Eq. (4).
2. Fix wave vector k, vary frequency ω with a small step, and look for changes in the sign of $\det[M]$. Then record the relation of $\omega\sim k$.
3. Transform the coordinate system from x,y,z to $u=z-s(x)$, $v=x$, $w=y$. For a TM polarization mode, the component of the electric field locally parallel to the surface $E_\parallel$ and that of the magnetic field normal to the symmetry H_y are re-expressed as

$$F=\left(\frac{\mu_0}{\varepsilon_0}\right)^{1/2}H_y,\quad G=-\frac{\omega}{c}\varepsilon E_\parallel\sqrt{1+s'^2}. \quad (7)$$

Then a system of partial differential equations can be derived from Maxwell's equations in a covariant form and the Floquet–Bloch theorem:

$$-i\frac{d\xi}{du}=[T]\xi(u), \quad (8)$$

where $\xi(u)=\lim_{N\to\infty}(F_{-N},F_{-N+1},\ldots,F_{N-1},F_N,G_{-N}/\varepsilon,\ldots,G_N/\varepsilon)$ is a generalized column vector. The coefficient matrix $[T]$ is also defined by the limit $N\to\infty$ of several assistant matrices and the detailed expression can be found in [23].

4. Substitute the relation of $\omega\sim k$ into coefficient matrix $[T]$ for each medium and calculate the eigenvalues λ^q and eigenvectors φ^q from $([T]-\lambda^q[I])[\varphi^q]=0$.
5. Calculate the expansion coefficients ξ_q in Eq. (8). The expansion coefficients ξ_q are proportional to the eigenvectors φ^q:

$$[\xi_q]=b_q[\varphi_q]. \quad (9)$$

Since the $\xi(u)$ is continuous at the boundary so that the proportional coefficient b_q in each medium can be calculated by a set of linear algebraic equations,

$$[\Phi^M][b^M]=[\Phi^D][b^D], \quad (10)$$

where $[\Phi^j],j=M,D$ is a matrix whose columns are the eigenvectors φ^q, and $[b_q^j],j=M,D$ is a column vector of proportional coefficients in the appropriate medium (metal and dielectric).

6. Calculate the coefficients for electromagnetic field component $E_\parallel$ and H_y. In order to obtain the field solution, we can write $[\xi_q]=\begin{bmatrix}f_m^q\\ g_m^q\end{bmatrix}$ and further convert the mode solution back to the rectangular coordinate system to obtain Eq. (6) and the mode solution for the electronic field:

$$E_\parallel(x,z)=-\frac{c}{\omega\cdot\varepsilon\cdot\sqrt{1+s'^2}}\sum_m\sum_q g_m^q\times\exp[i\lambda^q(z-s(x))]\exp\left[i\left(k+m\frac{2\pi}{a}\right)x\right]. \quad (11)$$

7. By Maxwell's equations, the component of the electric field locally normal to the surface calculation E_N can be calculated as

$$E_N(x,z) = \frac{1}{\omega \cdot \varepsilon \cdot \sqrt{1+s'^2}} \frac{\partial H_y}{\partial y}, \tag{12}$$

or the components of the electric field along the x and z directions E_x, E_z can be calculated as

$$E_x(x,z) = -\frac{i \cdot c}{\omega \cdot \varepsilon} \cdot \frac{\partial H_y}{\partial z}, \tag{13.a}$$

$$E_z(x,z) = \frac{i \cdot c}{\omega \cdot \varepsilon} \cdot \frac{\partial H_y}{\partial x}. \tag{13.b}$$

Therefore, a combination method to solve the normal SPP mode propagating on a cylindrical periodic dielectric-metal interface is set up by taking advantage of GFM and CDA. In the following section we will present some examples and discuss the calculation details.

3. CALCULATION OF SPP MODE ON PERIODIC INTERFACE

In this section, the field and surface charge distributions of an SPP mode propagating on an Au-Si_3N_4 interface are calculated by using the proposed combination method. The permittivity of Au-Si_3N_4 is assumed as $\varepsilon_D = 4$, while the dielectric function of Au is obtained by the data in [24] and fitted as a Drude model:

$$\varepsilon_{Au}(\omega) = \varepsilon_\infty \left[1 - \frac{\omega_p^2}{\omega^2}\right], \quad h\omega_p = 2.87 \text{ eV}, \quad \varepsilon_\infty = 8.9. \tag{14}$$

A. Results at First Brillouin Zone Boundary with Sinusoidal Interface Shape

First, the interface profile was set as sinusoidal function $s(x) = d \cdot \sin(2\pi/ax)$, while the period and depth were $a = 100$ nm and $d = 5$ nm, respectively. For calculating the dispersion curve, the order of coefficient matrix $[M_{m,n}]$ was set as $11(N=5)$ and the frequency searching step was set as $\omega_{step} = 0.001$ eV.

The calculated dispersion curves are plot as solid circles in Fig. 3. As reference, the light line in dielectric (Si_3N_4) and dispersion curve of the flat Au-Si_3N_4 interface are also plotted in solid and dashed lines, respectively. The energy band gap can be observed clearly. There are two branches for the dispersion curves of the sinusoidal shaped interface, while one is higher than that of the flat interface and the other is lower. Meanwhile, all of the dispersion curves are under the light line. Moreover, the frequencies of SPP modes at the Brillouin zone boundary ($k_x = K_g/2 = \pi/a = 3.14 \times 10^7$ m^{-1}) are also calculated by using the analytical formulation in [16] and shown as hollow diamonds in Fig. 3. As expected, the mode frequencies at $k_x = \frac{K_g}{2}$ of the numerical and analytical solutions are consistent.

Following steps 3–7 in Section 2, the calculated dispersion curves were applied for calculating the electromagnetic field distribution based on CDA. Here the order of coefficient matrix $[T]$ was set as 3 ($N=1$) and the proportional coefficient b_q was obtained by solving Eq. (10) with

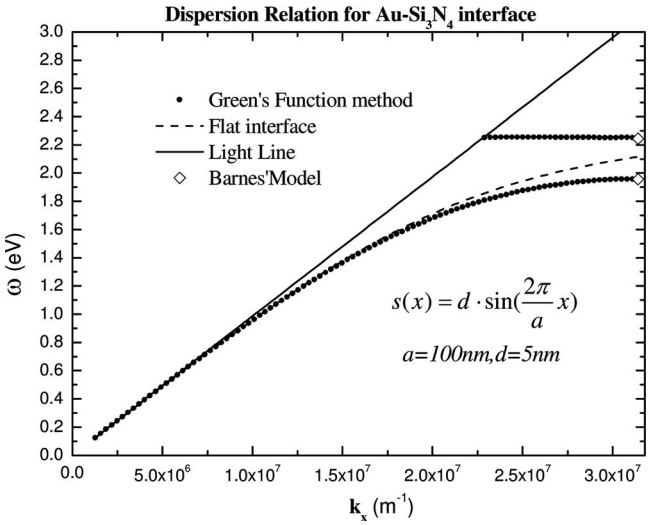

Fig. 3. Calculated dispersion curves for Au-Si_3N_4 interface with sinusoidal shape (period $a = 100$ nm and depth $d = 5$ nm). Here the light lines in dielectric and dispersion curve of flat Au-Si3N4 interface are also plotted in solid and dashed curves, respectively.

the least square method. The spatial region in calculation was divided to 201×201 mesh grids along the x and z axes with the range of 25 nm $\leq x \leq$ 225 nm and -100 nm $\leq z \leq 100$ nm. The calculated field intensity of H_y, $E_\parallel$ and E_N at $k_x = \frac{K_g}{2}$ are shown in Fig. 4 in a contour map, where all the intensities are normalized by the maximum value on the boundary, and regions of high field strength are shown as white.

As mentioned by Barnes [16], the physical origin of the SPP band gap can be found from the fact that two standing wave solutions of SPP modes, with different dispersion curves shown in Fig. 3, take different positions with respect to the peaks and troughs of the interface. Such conclusion is also confirmed by our calculation results shown in Fig. 4. It can be observed clearly that the extremum of each field component occurs at the peaks or troughs. For the lower frequency mode, shown in Figs. 4(a)–4(c), the surface charge distribution should be concentrated around the peaks so that the extremum of normal field component E_N occurs at the same position, whereas the extremum of both H_y and $E_\parallel$ is around the troughs. For the higher frequency mode shown in Figs. 4(d)–4(f), E_N will occur at troughs. These calculation results are similar to those in [4].

To verify our calculation more, the results of field distributions at the interface are compared to those calculated by the analytical formulation in [16]. Here, only the results of H_y combined with the spatial distribution of the interface are shown in Fig. 5, where the gray circles and the black solid lines are obtained by numerical calculation and analytical formulation, respectively. From them, different standing wave distributions of two SPP modes can be observed also, and all of them are well consistent with those from the analytical formulation. In addition, by comparing the field distributions of the low-frequency mode (Fig. 4(a)) to the high-frequency mode (Fig. 4(d)), it can be easily found that the energy of the lower frequency mode is more concentrated to the metal, while that of the higher frequency mode is to the dielectric. This phenom-

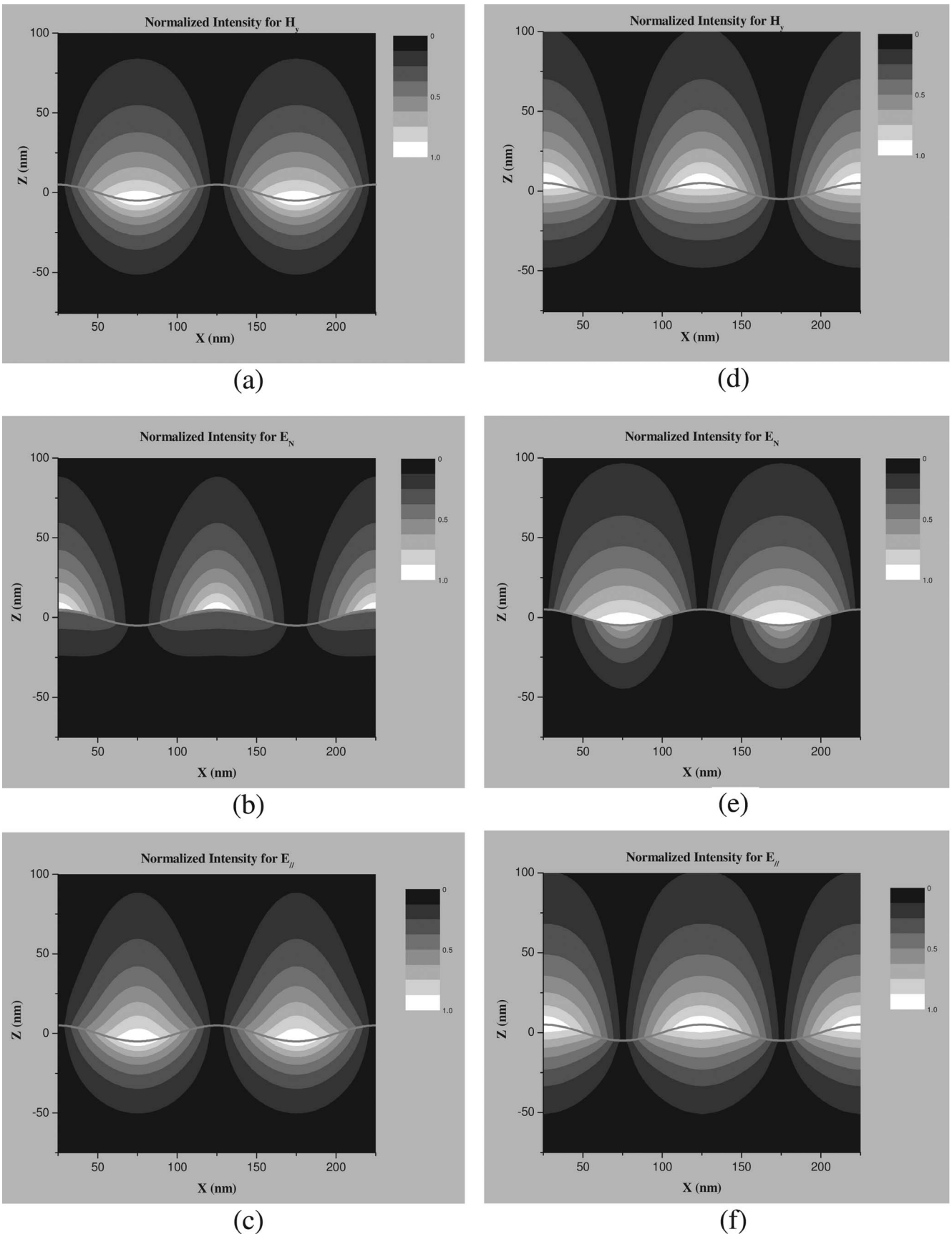

Fig. 4. (a) Normalized spatial distribution of the magnetic field normal to symmetry $|H_y|$, (b) electric field locally parallel to surface $|E_{\|}|$, (c) normal to surface $|E_N|$ for low-frequency mode and (d)–(f) those for high frequency modes at the first Brillouin zone boundary ($k_x = K_g/2$). The regions of high field strength are shown as white.

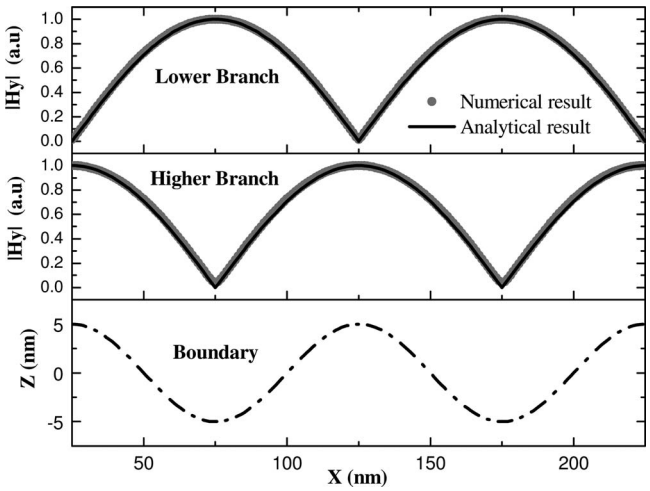

Fig. 5. Comparison of $|H_y|$ field distribution at interface between our numerical calculation (gray circles) and analytical formulation in [16] (black solid lines).

enon can be explained in that the higher frequency branch is pushed closer to the light line so that more energy of the SPP field is "shifted" to the dielectric side of interface [16].

B. Field Distribution Along Whole Dispersion Curve

Calculation results of SPP field distribution shown in Subsection 3.A are all for the first Brillouin zone boundary $\left(k_x=\frac{K_g}{2}\right)$. They identify with those reported by Barnes in [16] and verify the correctness of our proposed combination method. By substituting the wave vector k_x and related frequency ω on the dispersion curve into the same calculating steps as those in Section 2, the field distribution at an arbitrary wave vector can be obtained. As an example, the field distributions at $k_x=0.5K_g, 0.38K_g, 0.25K_g, 0.05K_g$ of the lower branch were calculated with the same conditions as Subsection 3.A, and the results of normalized $|H_y|$ are shown in Figs. 6(a)–6(d). It can be observed that a difference of field strength at troughs and peaks of the interface decrease while reducing the wave vector. When $k_x=0.05K_g$, the curve is almost flat, which can be observed more clearly from $|H_y|$ distributions at interface as shown in Fig. 7. This fact can be easily understood as follows. At the Brillouin zone boundary $\left(k_x=\frac{K_g}{2}\right)$, the two spatial waves propagating in opposite directions can perfectly interfere with each other so that the standing wave distribution of the SPP mode is generated. With the wave vector of the SPP mode decreasing, only partial interference can occur and the field strength at troughs and peaks close up. When $k_x=0.05K_g$, the wavelength of the SPP mode is much longer than the period of interface so that the field distribution is not nearly as affected by the interface corrugation and is close to that on the flat metal–dielectric interface.

C. Symmetrical Sawtooth Shape

In the above two sections, the simplest case that profiles a metal–dielectric interface in a sinusoidal shape has been discussed. In principle, both GFM and CDA can be used to arbitrarily shape function so that the proposed combination method can also be applied. As an example, the SPP mode solution will be discussed on the interface with a symmetrical sawtooth shape as follows.

The interface is still assumed as Au-Si_3N_4. The shape function was set as an odd symmetrical form:

$$s(x)=\begin{cases} h+\dfrac{4h}{a}\left(x-ma-\dfrac{a}{4}\right), & -\dfrac{a}{2}\le x-ma-\dfrac{a}{4}\le 0 \\ h-\dfrac{4h}{a}\left(x-ma-\dfrac{a}{4}\right), & 0\le x-ma-\dfrac{a}{4}\le\dfrac{a}{2} \end{cases} . \tag{15}$$

The values of h and a were assumed as $h=5$ nm and $a=100$ nm, respectively.

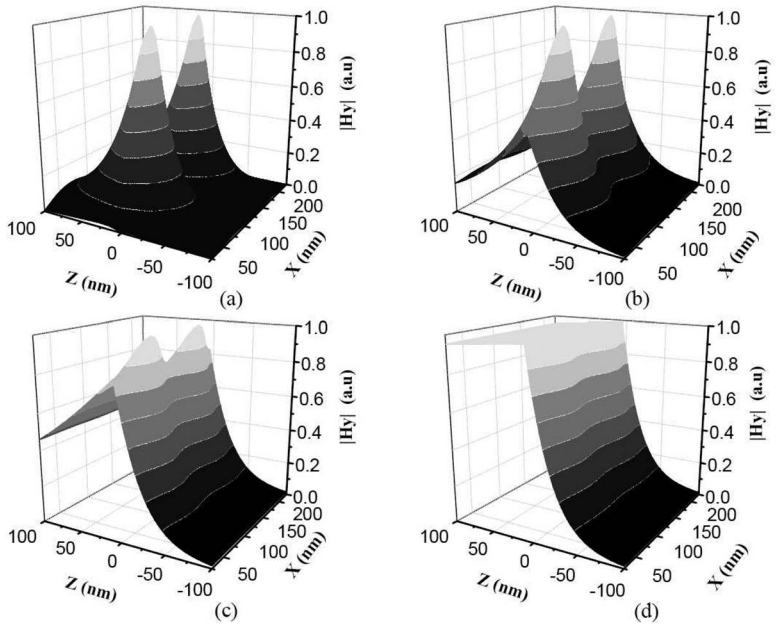

Fig. 6. Normalized field distributions of $|H_y|$ for the lower branch at (a) $k_x=0.5K_g$, (b) 0.38 K_g, (c) 0.5 K_g, and (d) 0.05 K_g.

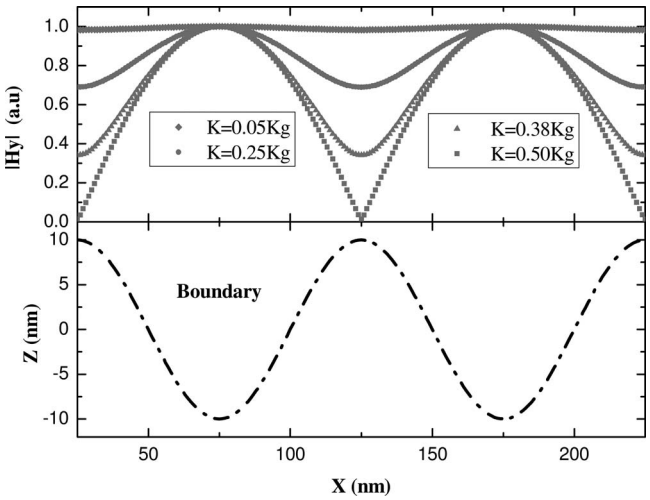

Fig. 7. Normalized field distributions of $|H_y|$ at interface for the lower branch at $k_x=0.5K_g$, 0.38 K_g, 0.5 K_g, and 0.05 K_g.

The dispersion curve was calculated by setting $N=5$, $\omega_{step}=0.001$ eV and is shown as gray circles in Fig. 8, where the black solid lines are those for sinusoidal shapes with the same depth and period. Comparing these dispersion curves, one can find that there is no significant difference, but the band gap of the sawtooth shape function is a little narrower. It can be explained as that the SPP band gap is most affected by the lowest harmonic component of the interface [16]. The dispersion curve is also calculated by setting the interface shape only with the first Fourier component of Eq. (15) and is shown as a black dotted line in Fig. 8. It can be observed that they are nearly the same as those for symmetrical sawtooth shape functions, and the maximum difference of the SPP frequency is less than 0.004 eV.

Then the field distributions of the SPP mode were calculated following the combination method. The results of

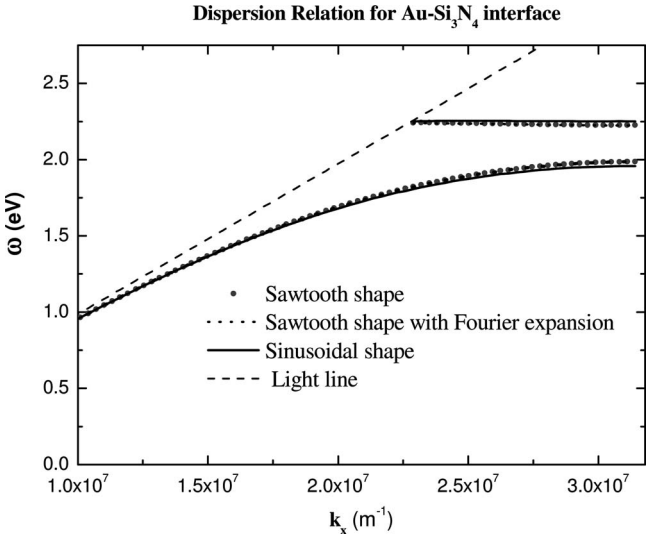

Fig. 8. Calculated dispersion curves for Au-Si_3N_4 interface with symmetrical sawtooth shapes (gray dotted line, period $a=100$ nm, and depth $d=5$ nm). Here black solid lines are for sinusoidal shapes with the same depth and period, and the black dotted lines are for the interface shapes only with the first Fourier component of Eq. (15).

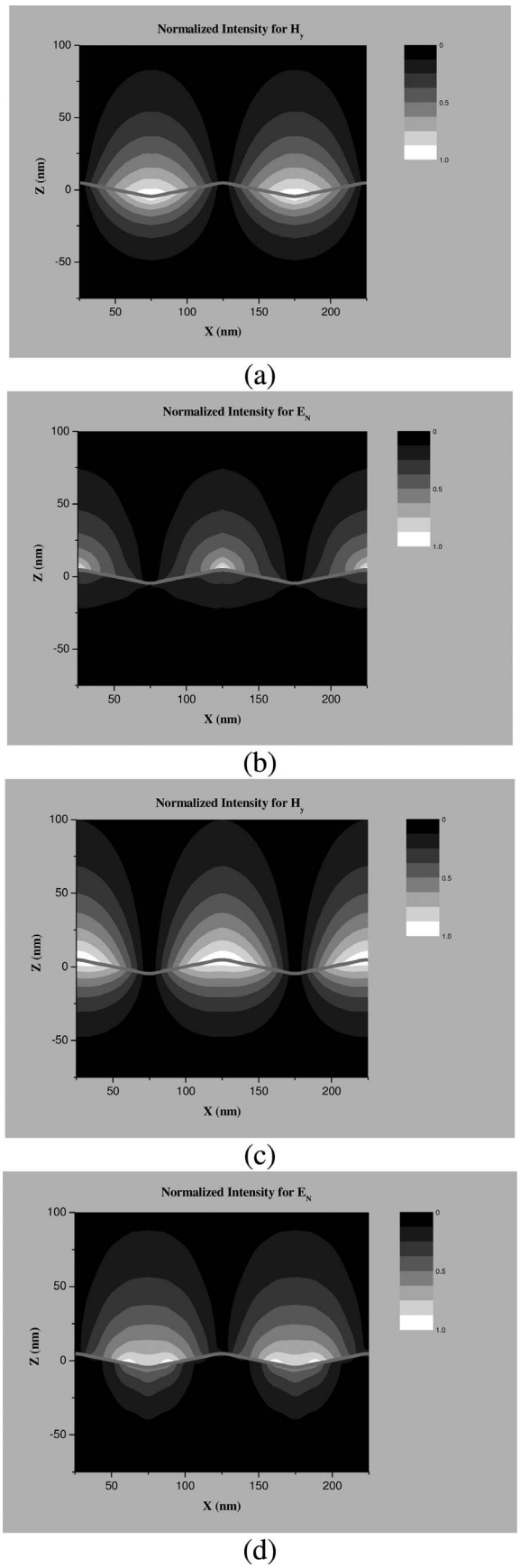

Fig. 9. Normalized spatial distribution of (a) $|H_y|$ and (b) $|E_N|$ for low-frequency mode and (c)–(d) those for high-frequency mode at $k_x=K_g/2$ with symmetrical sawtooth shapes.

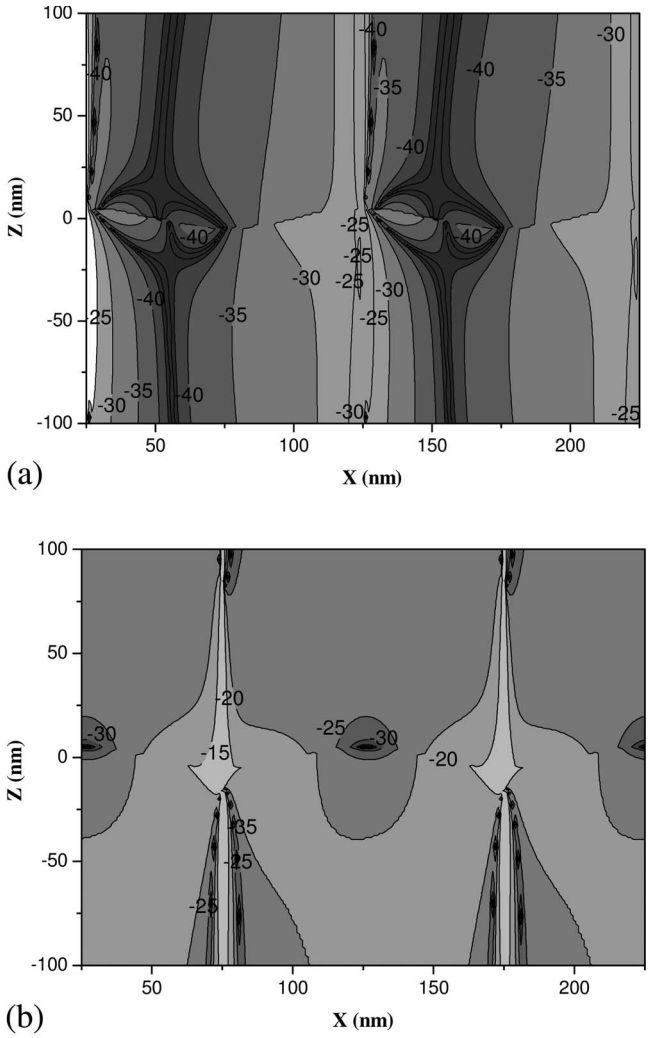

Fig. 10. Calculated variation of $|H_y|$ field intensity ($\Delta = 10\log_{10}\{2\cdot abs(|H_y^1|-|H_y^2|)/|H_y^1|+|H_y^2|\}$) for (a) low-frequency mode and (b) high-frequency mode by setting the frequency searching step $\omega_{step}=0.001$ eV and $\omega_{step}=10^{-5}$ eV with sinusoidal shape interface the same as Fig. 4.

$|H_y|$ and $|E_N|$ at $k_x=\frac{K_g}{2}$ are shown in Figs. 9(a)–9(d) for lower and higher frequency modes, respectively. Comparing them to the results for sinusoidal shapes in Figs. 3(a), 3(b), 3(d), and 3(e), one can find that the strength distribution of the $|H_y|$ field is very similar, but that of $|E_N|$ is different. The white regions in Figs. 9(b) and 9(d) are much narrower than those in Figs. 3(b) and 3(e) and more concentrated around the peaks or troughs. It indicates that the surface charges are more concentrated due to sharper ends of the sawtooth shape interface.

From the results mentioned above, we can find that the dispersion curves of the SPP mode are mainly determined by the lowest harmonic of the interface shape, but the field distributions are evidently influenced by the higher harmonic.

D. Calculating Stability of Proposed Combination Method

Until now, it has been proved that the proposed combination method could be adapted to calculate the electromagnetic field distribution for arbitrary wave vectors and arbitrary interface shape functions. The valid range of corrugated amplitudes for GFM and CDA has been discussed by many authors [1,2,6,16,20,23]. So, such a discussion is not included in this paper, and we will discuss how the calculation results of field distribution depend on the accuracy of dispersion curves in this section.

We selected the frequency searching step $\omega_{step}=0.001$ eV and $\omega_{step}=10^{-5}$ eV to investigate how the calculation results of electromagnetic field distribution vary with the dispersion curves obtained from two such different values of ω_{step}. Here we use a parameter Δ to evaluate such difference, which is defined as

$$\Delta = 10\log_{10}\left\{2\cdot\frac{abs(|H_y^1|-|H_y^2|)}{|H_y^1|+|H_y^2|}\right\}. \quad (16)$$

Figs. 10(a) and 10(b) show the results at $k_x=\frac{\pi}{a}$ for lower and higher energy SPP modes, respectively, where the darker color represents smaller value of Δ and only the values of $\Delta > -40$ dB are indicated. Compared with Fig. 4(a), it can be observed in Fig. 10(a) that, for the lower frequency mode, Δ is less than -40 dB in most parts of the region around the troughs of the interface ($X=75,175$ nm), while larger Δ appears only in the region around the peaks of the interface ($X=0,125,225$ nm) where the strength of $|H_y|$ is nearly equal to 0. Here, the larger value of Δ can be considered as an error due to subtraction between two real numbers near zero. The situation is similar for higher frequency modes, and the value of Δ is less than -25 dB in most parts around the peaks where $|H_y|$ is more concentrated. It is clear that for both SPP modes $\omega_{step}=0.001$ eV is sufficient, because the field distribution of the SPP mode is changed less than 0.3% ($\Delta=-25$ dB) as ω_{step} is increased to $\omega_{step}=10^{-5}$ eV. A moderate frequency step and coefficients matrix order guarantee that the proposed combination method has quite good stability for calculating the normal mode solution of SPP propagating on a spatial periodic interface.

4. CONCLUSIONS

By taking advantage of GFM and CDA, a numerical combination method is proposed for calculating the electromagnetic field distribution of the SPP mode on a cylindrical periodic dielectric–metal interface. Here, the dispersion curves are calculated following the GFM, and the electromagnetic field distributions are obtained by applying the two-dimensional field expansion form of CDA. With the proposed method, it is demonstrated that dispersion curves of a metal–dielectric interface with arbitrary shapes such as sinusoidal and symmetrical sawtooth shapes can be calculated. Meanwhile, the electromagnetic field distribution can be well calculated not only at the first Brillouin zone boundary $\left(k_x=\frac{K_g}{2}\right)$ but also at an arbitrary wave vector along the dispersion curve. As examples, the dispersion curves and electromagnetic field distributions of the SPP mode are presented based on an Au-Si_3N_4 interface with sinusoidal and symmetrical sawtooth shapes. By comparing the field distributions obtained with different frequency searching steps, it is proved that the proposed method has quite good stability.

The variation of field intensity is less than 0.3% as ω_{step} increased from 0.001 eV to 10^{-5} eV for the sinusoidal interface shape.

Since the dispersion relation of SPP modes as well as their field distributions can be well calculated, the proposed method in this paper provides a useful tool for research related to the local SPP field strength in areas such as the nonlinear effects in SPP crystals and quantum electrodynamics effects, especially for spontaneous emission lifetime modification.

ACKNOWLEDGMENTS

This work is supported by the National Basic Research Program of China (973 Program) under contract 2007CB307004. The authors thank Fang Liu and Yuxuan Wang and for their valuable discussions and helpful comments.

REFERENCES

1. *Electromagnetic Surface Excitations*, R. F. Wallis and G. I. Stegeman, eds. (Springer Series on Wave Phenomena, 1986), Vol. 3.
2. A. V. Zayatsa, I. I. Smolyaninovb, and A. A. Maradudinc, "Nano-optics of surface plasmon polaritons," Phys. Rep. **408**, 131–314 (2005).
3. J. D. Joannopoulos, R. D. Meade, and J. N. Winn, *Photonic Crystals* (Princeton U. Press, 1995).
4. W. L. Barnes, T. W. Preist, S. C. Kitson, J. R. Sambles, N. P. K. Cotter, and D. J. Nash, "Photonic gaps in the dispersion of surface plasmon on gratings," Phys. Rev. B **51**, 11164–11167 (1995).
5. W. L. Barnes, S. C. Kitson, T. W. Preist, and J. R. Sambles, "Photonic surfaces for surface-plasmon polaritons," J. Opt. Soc. Am. A **14**, 1654–1661 (1997).
6. *Surface Polaritons*, V. M. Agranovich and D. L. Mills, eds. (North-Holland, 1982).
7. W.-C. Tan, T. W. Preist, J. R. Sambles, and N. P. Wanstall, "Flat surface-plasmon-polariton bands and resonant optical absorption on short-pitch metal gratings," Phys. Rev. B **59**, 12 661–12 666 (1999).
8. B. Wang and G. P. Wang, "Plasmon Bragg reflectors and nanocavities on flat metallic surfaces," Appl. Phys. Lett. **87**, 013107 (2005).
9. M. Kreiter, S. Mittler, and W. Knoll, "Surface plasmon-related resonances on deep and asymmetric gold gratings," Phys. Rev. B **65**, 125415 (2002).
10. F. Liu, Y. Rao, Y. D. Huang, D. Ohnishi, W. Zhang, and J. D. Peng, "A novel LRSPP based refractive index sensor," in Proceedings of International Symposium on Biophotonics, Nanophotonics and Metamaterials (IEEE, 2006), pp. 103–105.
11. N. F. Chiu, S. Y. Nien, C. Yu, J. H. Lee, and C. W. Lin, "Advanced metal nanostructure design for surface plasmon photonic bandgap biosensor device," in Annual International Conference of the IEEE Engineering in Medicine and Biology (EMBS'06) (IEEE, 2006), pp. 6521–6524.
12. K. Okamoto, I. Niki, A. Shvartser, Y. Narukawa, T. Mukai, and A. Scherer, "Surface-plasmon-enhanced light emitters based on InGaN quantum wells," Nature Mater. **3**(9), 601–605 (2004).
13. I. Gontijo, M. Boroditsky, and E. Yablonovitch, "Coupling of InGaN quantum-well photoluminescence to silver surface plasmons," Phys. Rev. B **60**, 11564–11567 (1999).
14. X. L. Hu, Y. D. Huang, W. Zhang, and J. D. Peng, "Dominating radiative recombination in a nanoporous silicon layer with a metal-rich Au (1-α)-SiO2(α) cermet waveguide," Appl. Phys. Lett. **89**, 081112 (2006).
15. W. L. Barnes, "Fluorescence near interfaces: the role of photonic mode density," J. Mod. Opt. **45**(4), 661–699 (1998).
16. W. L. Barnes, T. W. Preist, S. C. Kitson, and J. R. Sambles, "Physical origin of photonic energy gaps in the propagation of surface plasmons on gratings," Phys. Rev. B **54**, 6227–6244 (1996).
17. T. Sφndergaard and S. I. Bozhevolnyi, "Vectorial model for multiple scattering by surface nanoparticles via surface polariton-to-polariton interactions," Phys. Rev. B **67**, 165405 (2003).
18. T. Søndergaard and S. I. Bozhevolnyi, "Surface plasmon polariton scattering by a small particle placed near a metal surface: an analytical study," Phys. Rev. B **69**, 045422 (2004).
19. T. Søndergaard and S. I. Bozhevolnyi, "Theoretical analysis of finite-size surface plasmon polariton band-gap structures," Phys. Rev. B **71**, 125429 (2005).
20. B. Laks, D. L. Mills, and A. A. Maradudin, "Surface polaritons on large-amplitude gratings," Phys. Rev. B **23**, 4965–4976 (1981).
21. M. Kretschmann and A. A. Maradudin, "Band structures of two-dimensional surface-plasmon polaritonic crystals," Phys. Rev. B **66**, 245408 (2002).
22. M. Kretschmann, "Phase diagrams of surface plasmon polaritonic crystals," Phys. Rev. B **68**, 125419 (2003).
23. J. Chandezon, M. T. Dupuis, and G. Cornet, "Multicoated gratings: a differential formalism application in the entire optical region," J. Opt. Soc. Am. **72**, 839–846 (1982).
24. *Handbook of Optical Materials*, M. J. Weber, ed. (CRC Press, 2003).